AIAA JOURNAL
Vol. 36, No. 2, February 1998

Neural-Network-Based Controller for Nonlinear Aeroelastic System

C.-S. Ku* and P. Hajela†
Rensselaer Polytechnic Institute, Troy, New York 12180

Attenuation of vibratory response is an important design consideration in many aeroelastic systems, and active methods of vibration reduction have been studied extensively in this context. Synthesis of active controllers requires that a good analytical model of the system be available. In those problems in which the aeroelastic system is inherently nonlinear, a robust control scheme is difficult to implement, particularly in the presence of large uncertainties in the model. The use of artificial neural networks, with on-line learning capabilities, is explored as an approach for developing robust control strategies for such problems. In particular, the use of neural networks to mimic the behavior of a linear quadratic Gaussian controller that is applicable to nonlinear systems is presented. The helicopter rotor blade is a classic example of an aeroelastic system in which vibration reduction is an overriding concern, and in which the plant is both nonlinear and contains uncertainties. A simplified two-dimensional representation of this aeroelastic system, consisting of an airfoil with a trailing-edge control flap, is considered as a test case in the present work; both structural and aerodynamic nonlinearities are included in the problem.

Nomenclature

a	= offset of elastic axis from the midchord
b	= semichord of airfoil
c	= distance between midchord and flap hinge
c_{mo}	= mean pitching-moment coefficient before stall
c_{ms}, c_{ps}	= static pitching-moment and lift coefficients, respectively
$c_{m\alpha}$, $c_{p\alpha}$	= slopes of linear pitching moment and lift curves, respectively
I_α, I_δ	= moments of inertia of airfoil and trailing-edge flap per unit span, respectively
K_α, K_h	= spring stiffnesses of torsional and translational restraints
m	= mass of airfoil per unit span
S_α, S_δ	= static moments of airfoil and trailing-edge flap per unit span, respectively
δ	= flap angle

I. Introduction

VIBRATORY response of helicopter rotor blades is generally computed through a complex, coupled analysis model, with contribution from the disciplines of structures, aerodynamics, and dynamics. This inherently nonlinear aeroelastic system frequently is represented by a linearized model, valid over a small range of operating conditions. An alternative approach is to develop linear identified models using experimental data from the physical nonlinear system. Detailed studies of such nonlinear aeroelastic systems have shown that the influence of nonlinearity is especially significant in computing the flutter speed and in determining the characteristics of flutter motions. Discounting the influence of nonlinearity also has been attributed as a cause for a number of unsuccessful attempts at vibration reduction using active control strategies.[1]

It is important, and indeed necessary, to compensate for nonlinear effects in the design of the controller. The most significant difference between nonlinear and linear systems is that the latter are amenable to the principle of superposition. Therefore, although the response of linear systems may be estimated by a standard test input, i.e., step input or ramp input, this approach is inapplicable in the presence of nonlinearities in the system. Additionally, for nonlinear systems, widely used techniques such as those based on Laplace or Z-transform analyses are also inapplicable, rendering the analysis more difficult.[2] For the nonlinear, unsteady aeroelastic system considered in this work, the controller not only must be able to provide fast response but also should exhibit adaptivity for varying operating conditions.

Gain scheduling is a control algorithm applicable to nonlinear systems. This approach changes the parameters of the controller by monitoring the operating conditions. The parameters of a linear controller for vibration reduction vary as a function of rotational speed of the rotor, and the rotor and fuselage vibration loads. A drawback of gain scheduling is that rapid changes in the plant dynamics when enlarging the flight operating range may render the gain scheduling controller ineffective for satisfying performance criteria.

The existence of plant uncertainties in this nonlinear system can cause a change in the dynamics during operation. In general, uncertainty may be defined as either a parametric uncertainty, an unstructured uncertainty, or unmodeled dynamics. Model reference adaptive control (MRAC) and sliding mode control are two nonlinear control schemes used to compensate for the effects of the plant uncertainty. MRAC applies a priori knowledge and adapts to the unmodeled part of the plant. This algorithm is able to compensate for the uncertainty by adjusting the plant parameters on-line. However, the issues of control-algorithm instability and the large computation time required for retuning the reference model because of the uncertainty still need be addressed.[3] Sliding mode control is insensitive to the changes of plant parameters and external disturbances. The basic idea of this control algorithm is to select a sliding surface in the state space and to force all states of the plant to achieve this chosen surface. However, some state variables are not available and the sliding surface is difficult to locate. Both shortcomings complicate the implementation of this approach.[4]

Robust control schemes, such as H_∞ optimal control, improve the performance of the system response and guarantee closed-loop stability. This approach has become one of the dominant control algorithms applied to helicopter vibration problems.[5] The concept of H_∞ optimization theory is to minimize the maximum singular value of the closed-loop frequency response function. A disadvantage in this approach is that, if specific values of the phase or gain margin are to be realized or if large variations in operating conditions are to be accommodated, it may be difficult to design the controller. A neural-network-based approach that overcomes these problems to a limited degree is proposed in Ref. 6. That work also underscores the limitations of the H_∞ controller in problems in which the nonlinearity is severe.

Received Feb. 28, 1997; presented as Paper 97-1182 at the AIAA/ASME/ASCE/AHS/ASC 38th Structures, Structural Dynamics, and Materials Conference, Kissimmee, FL, April 7–10, 1997; revision received Sept. 30, 1997; accepted for publication Oct. 20, 1997.

*Research Associate, Department of Mechanical Engineering, Aeronautical Engineering and Mechanics. Member AIAA.

†Professor, Department of Mechanical Engineering, Aeronautical Engineering and Mechanics. Associate Fellow AIAA.

The present paper describes an alternative neurocontrol strategy that can better accommodate higher levels of nonlinearity in the plant; it is based on representing the deviation between a nominal linearized plant and the true nonlinear plant as a system disturbance. Such a neurocontroller provides real-time response and has the ability to learn complex dynamics incorporating uncertainty. It utilizes both adaptive-training and learning-training processes to identify and control a dynamic system. In practice, the adaptive-training controller allows for fast changes of the plant parameters and is capable of dealing with highly nonlinear systems over a wide range of parameter changes.

Subsequent sections of this paper describe the aeroelastic system and the structural and aerodynamic nonlinearities that are included in the model. The synthesis of a neurocontroller that delivers the desired performance and is able to account for plant uncertainties also is presented. This includes a brief introduction to the backpropagation neural network.

II. Aeroservoelastic Problem

A simplified two-dimensional representation of a helicopter rotor blade under periodic loading, which includes both structural and aerodynamic nonlinearities, was used as the aeroelastic system for which vibration attenuation was desired. The extension of Theodorsen/Greenberg aerodynamics presented in Ref. 7 was used to develop unsteady airloads for a two-dimensional airfoil with a trailing-edge flap (Fig. 1). The model is highly coupled with respect to both structural and aerodynamic parameters, and the equations of motion in terms of the plunge degree of freedom h and pitch degree of freedom α can be expressed as follows:

$$\ddot{\alpha} I_\alpha + \ddot{\delta}[I_\delta + b(c-a)S_\delta] + \ddot{h}S_\alpha + (1+n\alpha^2)\alpha K_\alpha = M_\alpha + M_s \tag{1}$$

$$\ddot{\alpha} S_\alpha + \ddot{\delta} S_\delta + \ddot{h}m + hK_h = P_L + P_s \tag{2}$$

where M_α and P_L are the unsteady pitching moment and lift force on the airfoil per unit span, respectively, obtained from the Theodorsen model. The terms M_s and P_s represent the pitching moment and the lift force about the midchord obtained from a dynamic stall model,[8] where

$$M_s = 2\rho b V^2 \Gamma_m + \tfrac{1}{2} b P_s \tag{3}$$

$$P_s = \rho b V \Gamma_p \tag{4}$$

The circulation variables Γ_m and Γ_p can be determined from the following second-order differential equations:

$$\ddot{\Gamma}_m + (V/b)z_{m1}\dot{\Gamma}_m + (V/b)^2 z^2 \Gamma_m = -z^2(V/b)^2 V \Delta c_m - z_{m2}\dot{w} \tag{5}$$

$$\ddot{\Gamma}_p + (V/b)z_{p1}\dot{\Gamma}_p + (V/b)^2 z^2 \Gamma_p = -z^2(V/b)^2 V \Delta c_p - z_{p2}\dot{w} \tag{6}$$

where Δc_m and Δc_p are the differences between the linear and the nonlinear static pitching moment and lift coefficients, respectively; they are both zero in the unstalled state. Also, w is the velocity of the flow normal to the airfoil (inflow velocity in rotor terminology) and a uniform value of $w = V/4$ is suggested[9] for the sake of simplicity.

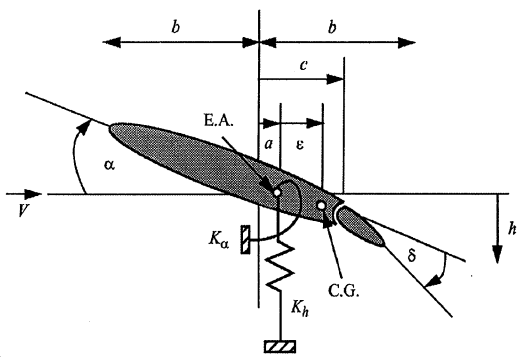

Fig. 1 Two-dimensional typical section.

The modification of Δc_m and Δc_p for large variations in angle α can be formulated as[10]

$$\Delta c_m = (c_{mo} + c_{m\alpha}\sin\alpha) - c_{ms} \tag{7}$$

$$\Delta c_p = c_{p\alpha}\sin\alpha\cos\alpha - c_{ps} \tag{8}$$

Values of $c_{m\alpha} = -0.001\ \text{rad}^{-1}$, $c_{p\alpha} = 2\pi\ \text{rad}^{-1}$, $c_{ms} = -0.01\ \text{rad}^{-1}$, $c_{ps} = 0.45\ \text{rad}^{-1}$, and $c_{mo} = 0.01\ \text{rad}^{-1}$, corresponding to a NACA 0012 airfoil, were used in all numerical simulations presented in this paper. The parameters z, z_{m1}, z_{m2}, z_{p1}, and z_{p2} are computed as follows:

$$z = 0.2 + 0.2(\Delta c_p)^2 \tag{9}$$

$$z_{m1} = 0.25 + 0.1(\Delta c_p)^2 \tag{10}$$

$$z_{m2} = 0.01(\Delta c_p)^2 \tag{11}$$

$$z_{p1} = 0.3 + 0.2(\Delta c_p)^2 \tag{12}$$

$$z_{p2} = -0.05(\Delta c_p)^2 \tag{13}$$

where the coefficients in Eqs. (9–13) are derived from measured data for a flat-plate airfoil. These coefficients are insensitive to the airfoil shape[8] and therefore can be used in this analysis. In Eq. (1), a structural nonlinearity is introduced by changing the linear torsional stiffness K_α to a form $K_\alpha(1 + n\alpha^2)$, where n is a constant that indicates the magnitude of the nonlinearity. Note that a hinge spring stiffness could be included in the equations of motion for the two-dimensional typical section but was neglected in the present work for the sake of simplicity. In forward flight, the airflow over the airfoil was considered to have a periodic time-varying behavior as

$$V = \Omega R(1 + \mu\sin\psi) \tag{14}$$

where Ω is the blade rotational speed, R is the rotor-blade radius, ψ is the azimuth angle, $\mu \equiv V_f/(\Omega R)$ is the tip speed ratio, and V_f is the forward speed of the helicopter. Note that in hover, $\mu = 0$, and therefore $V = \Omega R$, and there is no azimuthal variation in velocity.

The basic difference between the fixed-wing and rotary-wing theories is in the wake modeling, which depends on a deficiency function $C(k)$, where $k \equiv (\omega b)/V$ is a reduced frequency. An approach using a Bode plot analysis to derive a Pade approximation of the deficiency function, for both fixed-wing and rotary-wing cases, has been proposed recently.[11] This allows for generating a finite state model of unsteady aerodynamic loads due to the oscillatory motion. Using the following Pade approximation for the deficiency function in the expression for lift:

$$C(k) \cong 0.5 + \frac{0.0476}{ik + 0.8} + \frac{0.0612}{ik + 0.261} + \frac{0.0147}{ik + 0.072} \tag{15}$$

and further defining $ik = s(b/V)$, the inverse Laplace transform can be applied to calculate the circulatory lift force in the time-domain as follows:

$$P_C(t) \cong -2\pi\rho V b\left(0.5Q(t) + \int_0^t \frac{V}{b}Q(\tau) \times \left\{0.0476\exp\left[-0.8\frac{V}{b}(t-\tau)\right] + 0.0612 \times \exp\left[-0.261\frac{V}{b}(t-\tau)\right] + 0.0147 \times \exp\left[-0.072\frac{V}{b}(t-\tau)\right]\right\} d\tau\right) \tag{16}$$

where P_C is the lift force from circulatory loads and Q is written as

$$Q = V\alpha + \dot{h} + b\left(\frac{1}{2} - a\right)\dot{\alpha} + \frac{T_{10}V\delta}{\pi} + \frac{T_{11}b\dot{\delta}}{2\pi} \tag{17}$$

where T_{10} and T_{11} are as defined by Theodorsen.[12] A similar expression can be obtained for the circulatory pitching moments. The first term of the integration in Eq. (16) is defined as

$$n_1 = \int_0^t \frac{V}{b}Q(\tau)0.0476\exp\left[-0.8\frac{V}{b}(t-\tau)\right] d\tau \tag{18}$$

and from the Leibnitz rule, this can be written as

$$\frac{\mathrm{d}}{\mathrm{d}t}n_1 = -0.8\frac{V}{b}n_1 + 0.0476\frac{V}{b}Q(t) \tag{19}$$

The other integration term in Eq. (16) can be transformed similarly to obtain the following set of three first-order differential equations:

$$\begin{bmatrix}\dot{n}_1\\ \dot{n}_2\\ \dot{n}_3\end{bmatrix} = \begin{bmatrix}-0.8 & 0 & 0\\ 0 & -0.261 & 0\\ 0 & 0 & -0.072\end{bmatrix}\begin{bmatrix}n_1\\ n_2\\ n_3\end{bmatrix} + \begin{bmatrix}0.0476\\ 0.0612\\ 0.0147\end{bmatrix}Q(t) \tag{20}$$

The total lift force and the pitching moment on the airfoil can be obtained by combining the noncirculatory and the circulatory parts.

Equations (1), (2), (5), and (6) in conjunction with Eq. (20) can be transformed into a set of nonlinear first-order differential equations as

$$\dot{X}(t) = F[X(t), U(t)]$$
$$\dot{Y}(t) = G[X(t), U(t)] \tag{21}$$

where

$$X = [\alpha \quad \dot{\alpha} \quad h \quad \dot{h} \quad n_1 \quad n_2 \quad n_3 \quad \delta \quad \dot{\delta} \quad \Gamma_m \quad \dot{\Gamma}_m \quad \Gamma_p \quad \dot{\Gamma}_p]^T$$
$$U = [\ddot{\delta}] \tag{22}$$
$$Y = [\alpha \quad h]^T$$

and $X(t), U(t)$, and $Y(t)$ represent the state, input, and output vectors, respectively. Equation (21) can represent either the nonlinear time-invariant aeroelastic system in hover motion or a nonlinear time-varying (NTV) aeroelastic system in forward flight. Note that the flap displacement could be used as an input in place of the acceleration; sensing either one of these parameters in a practical implementation poses no significant problem.

Typical open-loop response of this nonlinear system due to a control surface input $U(t) = \sin(3\pi t)$ is shown in Figs. 2 and 3. This is simply the response of the system to a sinusoidally varying flap acceleration. Figure 2 shows how the pitch angle and the transverse displacement change with time for two different levels of spring nonlinearities and shows that the system has a divergent trend. Note that higher values of n result in an attenuation of the amplitude of the response. Figure 3 shows the open-loop response for both the NTV system and an approximate linear time-invariant (LTI) model established around the shown operating condition. The periodic nature of the response from the NTV model is due to the azimuthal variation in the velocity brought about by the addition of velocity components corresponding to the blade rotation and the forward

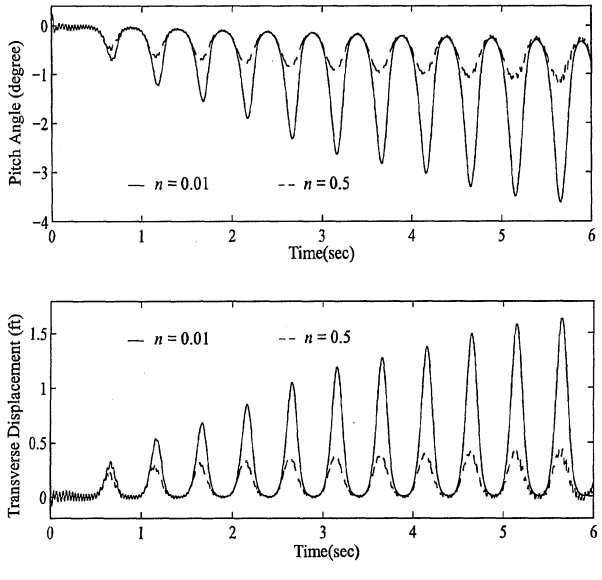

Fig. 2 Open-loop response of the NTV model (ΩR = 450 ft/s).

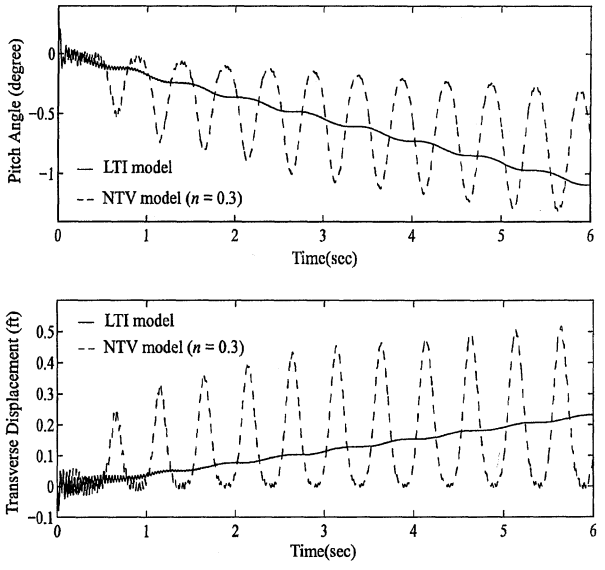

Fig. 3 Open-loop response of the NTV and LTI models (ΩR = 450 ft/s).

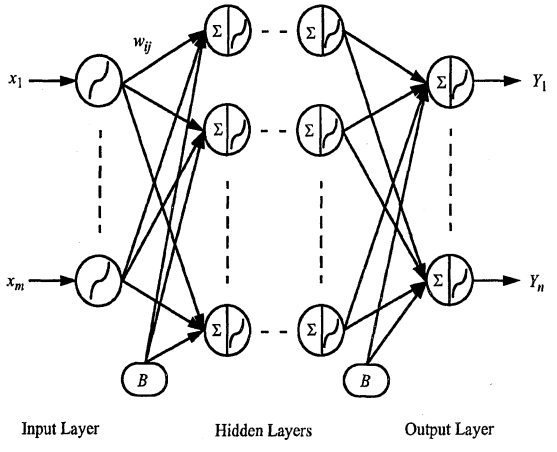

Fig. 4 Architecture of the multilayer perceptron.

speed of the helicopter; the period of this response is directly related to the rotational frequency of the blade. Changing operating conditions such as variations in blade rotation rate or forward speed of the helicopter significantly alter the behavioral response, and an active control system would be of some value in improving the overall system performance.

III. Multilayer Feedforward Neural Networks

Before we introduce the use of neural networks to develop a control strategy for the above problem, it is important to say a few words about what neural networks are and, in particular, how they are applicable to the present problem. The multilayer perceptron or the backpropagation neural networks[13] provide the ability to model complex, nonlinear, stable continuous functions with an arbitrary degree of accuracy. A detailed description of this network is beyond the scope of this paper. It suffices to say that the network architecture consists of a layer of artificial neurons to which the external stimuli are presented, a series of hidden layers of artificial neurons, and a layer of neurons at which the output is available (Fig. 4). Neurons in each layer are connected to all neurons in adjacent layers; there is an interconnection weight associated with this connection, which defines the strength of the connection. Also associated with each artificial neuron (excluding the input-layer neurons) is an activation function. The weighted sum of all inputs to a particular neuron are processed through this nonlinear activation function to produce a neuron output. A process referred to as network training simply requires the determination of all interconnection weights of the network and characteristics of all activation functions, so that

the network accurately produces the desired output for each of the input patterns used in the training. Once such a trained network is established, it responds to a new input within the domain of its training by producing an estimate of the output response. In the present work, a sigmoidal activation function was used for all neurons.

A trained neural network can be used in lieu of an analytical model of the plant. Alternatively, a network may be trained to map the inverse relationship of a plant and then used in series with the plant to provide a tracking control. A more powerful use of the neural network is to train the network to mimic the output of an optimal controller such as a linear quadratic Gaussian (LQG) controller and to use this in place of the LQG for real-time response. The manner in which the training patterns are provided to the network is an important consideration. Note that, in this feedback control system, both the feedback signal Y and the control signal U are functions of time. One approach to training a neural network with such time-dependent data, referred to as the learning-training approach, is to represent the continuous time-varying signals in a discrete manner. The size of the neural network in this case would correspond to the number of intervals in which the time period of interest is discretized. Clearly, the smaller time step will produce a better approximation to the continuous signal but also will result in increased network size and hence increased computational costs.

An alternative approach for network training, and the one actually used in this work, is the adaptive-training strategy. In this technique, only the feedback signal at the current time step is required in addition to the feedback and control signals at a few preceding time steps. Thus, the control signal $U(k)$ at time step k is obtained as

$$U(k) = f[Y(k), Y(k-1), Y(k-2)\cdots Y(k-m)U(k-1), U(k-2)\cdots U(k-i)] \tag{23}$$

where f represents the mapping relation and m and i represent the number of preceding time steps at which the feedback and control signals are required, respectively. The ability to create a good approximation depends on the selection of m and i. In practice, m and i are small integers (typically 2 or 3).[14] Note that, because the training in this work is performed off-line, there is ample scope for experimentation in the selection of m and i to ensure that the network provides a good function approximation. The architecture of the neural network is also dependent on the integers m and i. As an example, for scalar Y and U, and values of m and i both selected as 2, we would have five input quantities mapping into one output. This would result in a neural network with five neurons in the input layer and one in the output layer. The number of hidden layers and neurons in these layers generally is determined by trial and error. However, a single hidden layer with one to two times the number of input-layer neurons generally is sufficient to create the required mapping. In all numerical studies reported in this paper, the timescale was discretized into intervals of 0.001 s, which was less than one-fifth of the smallest period of the model under study.

IV. Neural-Network-Based Control System

For the aeroelastic problem considered here, the response computed from the linear approximate model is significantly different from that predicted by the nonlinear model, particularly at higher values of the dynamic pressure. A control approach that is applicable over a wide range of variations in system behavior is based on the use of a neural network to model the deviation between the outputs of the nonlinear plant and its linearized counterpart and to represent the deviation as a disturbance to be removed from the output of the nonlinear plant during operation.

As a first step in this problem, a linearized model of the plant is first established. Two forms of linear models can be considered. The first is an LTI model in which no spring hardening or dynamic stall effects are considered and for which there is no azimuthal variation in velocity. This corresponds to a case of hovering flight. The inclusion of forward flight in this model results in a linear, periodic time-varying (LTV) model. The present work focuses on the LTI model for which a commonly used control strategy is the LQG approach and for which the state-space representation is of the following form:

$$\dot{X}(t) = AX(t) + BU(t)$$
$$Y(t) = CX(t) \tag{24}$$

Here, $X(t)$, $U(t)$, and $Y(t)$ are defined as Eq. (22) and the time-invariant matrices A, B, and C are of appropriate dimensions.

If the principal objective of the controller synthesis problem is to simultaneously reduce the control effort and the system deflections denoted by the state variables, a quadratic performance index may be formulated as follows:

$$J = \int_0^\infty \left[X(t)^T Q_C X(t) + U(t)^T R U(t)\right] \mathrm{d}t \tag{25}$$

where Q_C and R are positive semidefinite and positive definite weighting matrices, respectively. These represent the weighting assigned to the state and control variables in the quadratic performance index. An optimal time-varying control input for such a system is obtained as

$$U(t) = -K(t)X(t) \tag{26}$$

where K is the gain computed from the equation

$$K(t) = R^{-1}B^T P(t) \tag{27}$$

and P is obtained as a solution of the algebraic Riccati equation as follows:

$$A^T P + PA - PBR^{-1}B^T P + Q = 0 \tag{28}$$

This well-known linear quadratic regulator (LQR) requires full state information, and is therefore difficult to implement in an on-line manner if some states are immeasurable. Furthermore, external disturbance or measurement noise degrades the performance of an LQR controller. An observer that uses system measurements to estimate the states may be combined with the LQR to improve overall performance. The use of a Kalman filter to obtain these estimates is particularly effective in the presence of noisy measurements. The combination of the LQR and the estimator yields the LQG control algorithm, and this approach has been implemented successfully in an LTI aeroelastic system by Takahashi and Friedmann.[15] Using a similar strategy, an LQG controller was established for the linear system in the present work. Furthermore, to improve the efficiency of the LQG controller for real-time implementation, it was possible to train a neural network to mimic the behavior of the LQG controller.

In the second step of the controller design, the control signal established for an LTI model for a given value of ΩR is applied to both the true aeroelastic model, i.e., NTV model, and the simplified linear model, i.e., LTI model. As shown in Fig. 5, this control signal and the deviation between the feedback signal from the NTV model Y_{non} and that obtained from the LTI model Y_{lin}, i.e., $Y_{\text{dev}} = Y_{\text{non}} - Y_{\text{lin}}$, are used as the I/O training patterns for another backpropagation neural network. When the error e between the neural-network-predicted

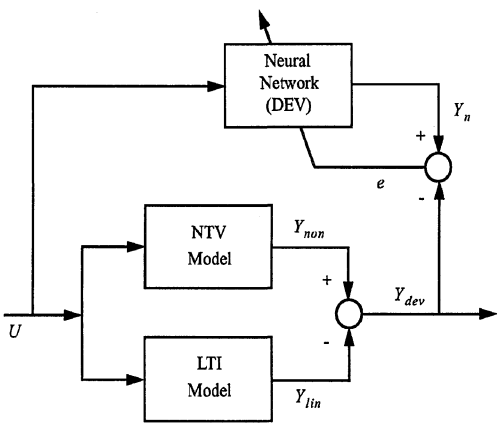

Fig. 5 Neural network identification of the system deviation.

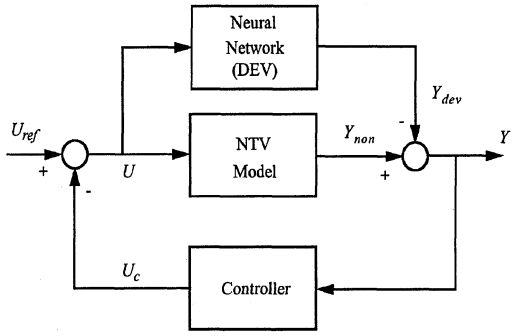

Fig. 6 Control block diagram for nonlinear aeroelastic system.

value Y_n and the deviation Y_{dev} is lower than a specific threshold, the training process is terminated. This trained neural network now represents the deviation Y_{dev} for a specific control signal U and is placed in the control loop as shown in Fig. 6. It is clear from this control loop diagram that the feedback signal the controller receives is exactly the signal for which it was designed. Indeed, placing the original nonlinear plant and the neural-network-modeled deviation in parallel as in Fig. 6, with the latter output treated as an external disturbance, is equivalent to controlling the linearized system.

Instead of the LTI model, an LTV model could have been used in the first step. A modified LQG controller, as described in Ref. 16, can be designed for such a plant. For a more extensive discussion of this approach, the reader may refer to Ref. 6.

V. Numerical Results

The synthesis of a neurocontroller for this nonlinear aeroelastic system was studied for a number of different flight conditions. For a case involving a rotational speed of 450 ft/s, a tip speed ratio of 0.3, and a value of $n = 0.3$, the deviations between the NTV and LTI aeroelastic systems are shown in Fig. 7. These deviations are significant and cannot be neglected or treated as a plant uncertainty. Indeed, as shown in Fig. 8, if the control signal corresponding to the LTI model is applied to the nonlinear system, the closed-loop response is less than satisfactory.

As a test problem, an LQG controller was synthesized using the LTI model. Numerical value of parameters used in this model are given as $a = -0.39$, $c = 0.645$, $m = 0.326$ slug, $K_\alpha = 583.6$ ft-lb, $K_h = 9928.0$ lb/ft, and $Q_C = 1700.0$. The adaptive-training process described in the Sec. IV was used to train a neural network to map the relationship between Y and U. This network consists of 8 neurons in the input layer, 12 neurons in the hidden layer, and 1 neuron in the output layer. In this case the feedback signal Y contains two components, α and h, and the control signal $U = \ddot{\delta}$ is a scalar. Values of $m = i = 2$ were found to create a good mapping, resulting in the aforementioned network architecture. A comparison of the control signal from an LQG controller and a trained neural network representing this controller is shown in Fig. 9. This is very little difference between these signals, attesting to a satisfactory network training.

To control the nonlinear system, a neural-network-based model of the deviations between the LTI and NTV models also was established. As shown in Fig. 5, the network must represent the mapping between the scalar U and the deviation in the two components of Y. Using the adaptive-training process, the control signal at a given time step and at two previous time steps, was used to predict the deviation in Y at the current time step. This resulted in a network architecture with 7 neurons in the input layer, 10 in the hidden layer, and 2 in the output layer. This trained neural network then was placed in parallel to the nonlinear system, as discussed earlier. The closed- and open-loop responses of the NTV model using the proposed approach are presented in Fig. 10. As shown by the closed-loop response, the structural deflections have been reduced as desired.

When the operating conditions such as the rotational speed of the blade change, the controller has to be redesigned. This is clearly depicted in Fig. 11, which shows the control effort corresponding

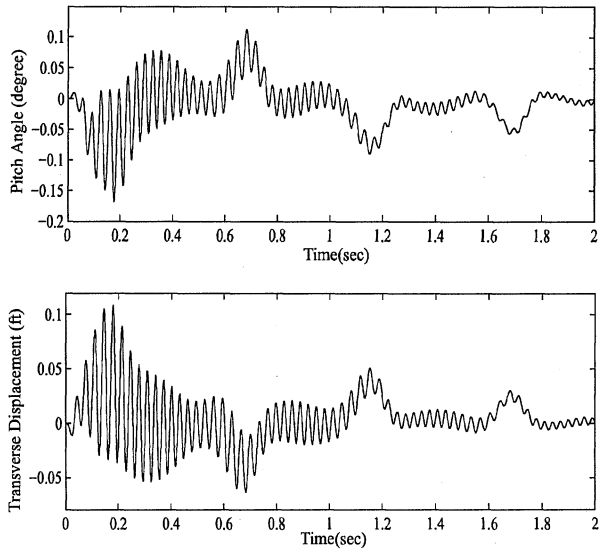

Fig. 7 Comparison of deviations between LTI and NTV models (ΩR = 450 ft/s).

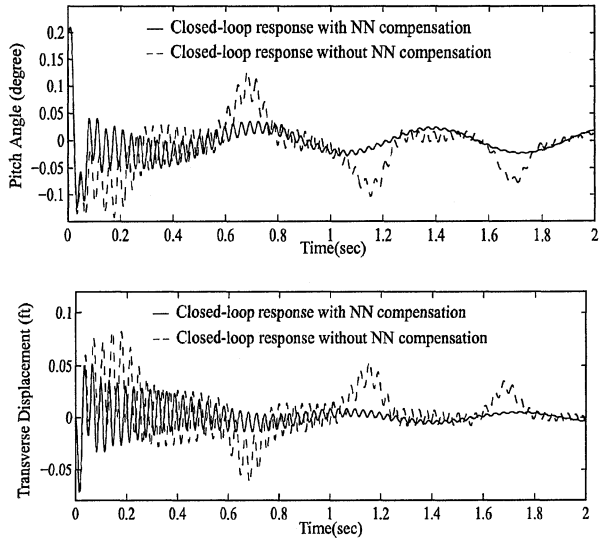

Fig. 8 Comparison of closed-loop response of NTV model with and without NN compensation (ΩR = 450 ft/s, n = 0.3).

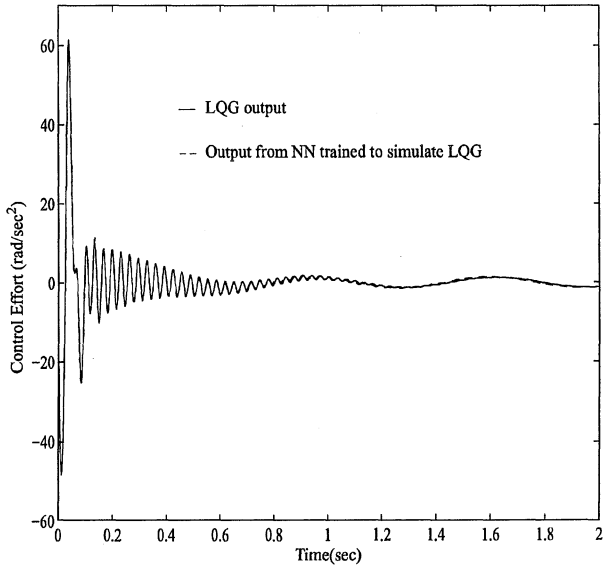

Fig. 9 Comparison of control signal predicted by LQG and an equivalent trained neural network (ΩR = 450 ft/s).

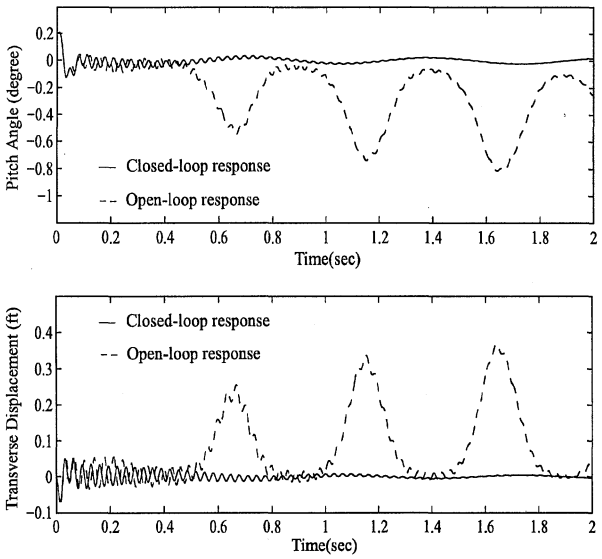

Fig. 10 Comparison of closed- and open-loop response of NTV model (ΩR = 450 ft/s).

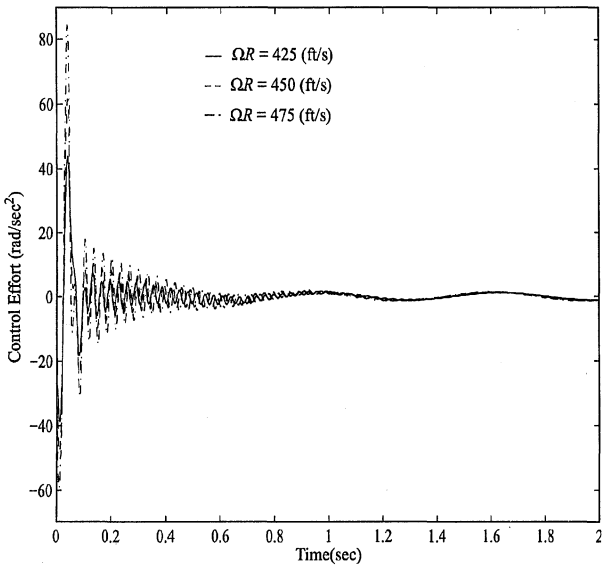

Fig. 11 Desired control signal for LTI model for different flight conditions.

to an LQG controller designed separately for three different rotational speeds. To accommodate this variation, two strategies are applicable. The neural network trained to mimic the LQG controller can have as an additional input the rotational speed. In this case, training data correspond to controller I/O signals for multiple rotational speeds, selected from within the operational envelope for the controller. In theory, such a controller, when presented with a new flight condition, would provide an interpolated output signal. To work satisfactorily, however, the controller would first have to be synthesized for several flight conditions. Alternatively, a few select rotational speeds can be prescribed, and the controller I/O data for these speeds can be used to train as many networks as there are rotational speeds. These trained networks then can be placed in parallel as shown schematically in Fig. 12, and for a new flight condition, an averaging process can be used to determine the control output. This approach has been successfully implemented and related results will be reported elsewhere. In the present work, the averaging was based on a metric distance between the rotational speed for which network response was desired, and the rotational speeds for which trained networks were available. If U_i is the output corresponding to a network trained for a rotational speed $(\Omega R)_i$, an averaged output $\bar{U}_d$ is obtained as

$$\bar{U}_d = \sum_{i=1}^{k} W_i U_i \tag{29}$$

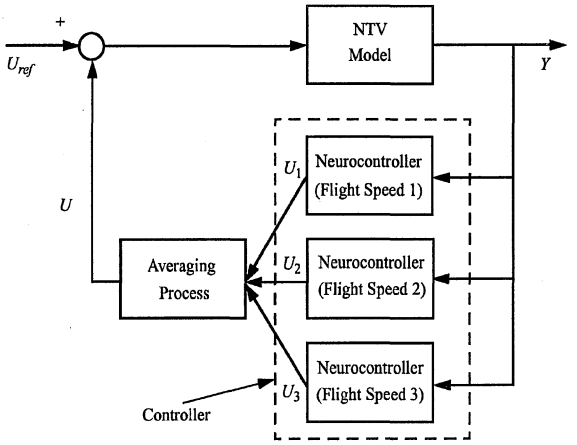

Fig. 12 Schematic showing the averaging process for the control signal.

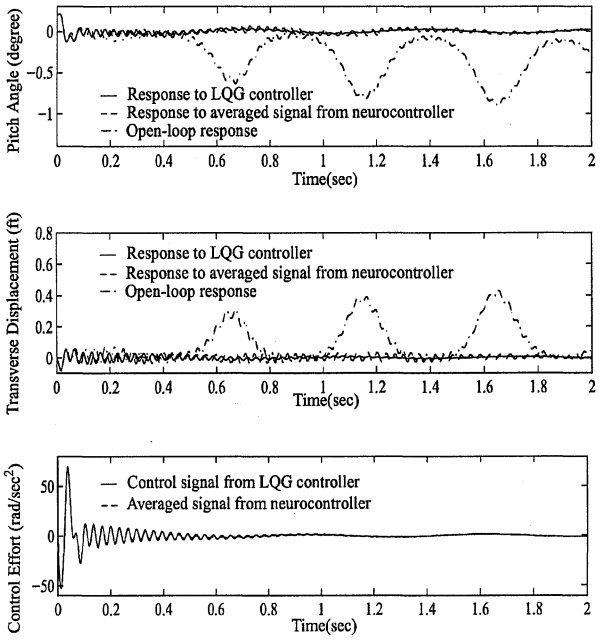

Fig. 13 Comparison of response and control signal under an LQG generated signal and a neural-network-averaged signal (ΩR = 460 ft/s, n = 0.3).

where

$$W_i = \left|\frac{1}{(\Omega R)_d - (\Omega R)_i}\right| \Bigg/ \sum_{i=1}^{k} \left|\frac{1}{(\Omega R)_d - (\Omega R)_i}\right| \tag{30}$$

Here, W_i is the computed weight and $(\Omega R)_d$ is the rotational speed for which an averaged output is required; k is the number of rotational speeds $(\Omega R)_i$ for which trained networks are available.

As an example, the performance of the neurocontroller for a new flight condition ΩR = 460 ft/s and tip speed ratio of 0.3, for which it was not trained, is summarized in Fig. 13. The control signal for this changed flight condition was obtained by aforementioned averaging process, using the control signals from three different neurocontrollers trained for rotational speeds of 425, 450, and 475 ft/s. Figure 13 shows a comparison of the averaged response and a response available from an LQG controller specifically designed for this new flight condition. Similar levels of performance were obtained when the averaging procedure was tested for other flight conditions, ranging from rotational speeds of 430 to 470 ft/s, attesting to the effectiveness of the neurocontroller over a wider operational range. A representative set of these results is shown in Table 1, where the deviations in the closed-loop response, obtained through the use of a redesigned LQG controller, and from an averaged control signal are presented as a time-averaged quantity.

Table 1 Time-averaged deviations between response due to a control signal from newly designed LQG controller and an averaged control signal

Flight condition (ΩR), ft/s	$(1/T)(\sum \lvert\Delta\alpha\rvert^2)^{0.5}$	$(1/T)(\sum \lvert\Delta h\rvert^2)^{0.5}$
430.0	0.1955	0.1407
440.0	0.3287	0.2393
460.0	0.4356	0.3445
470.0	0.3668	0.2905

VI. Conclusions

The development of a neural-network-based control strategy for nonlinear dynamic systems is described. A simple aeroelastic model is considered for control and includes both structural and aerodynamic nonlinearities. A neural-network-based procedure to identify and model the deviations between the actual nonlinear system and a simplified linear model and to represent this deviation as a disturbance to be rejected forms the basis for the neurocontroller strategy. An LQG controller is shown to provide satisfactory performance. The paper also shows that the control signal from different neurocontrollers, each applicable to a different operating condition can be averaged to provide an appropriate control signal for a new flight condition.

Acknowledgment

Support received from the Army Research Office under Research Grant DAAH-04-93-G-0003 to the Rensselaer Rotorcraft Technology Center is gratefully acknowledged.

References

[1]Molusis, J. A., Mookergee, P., and Bar-Shalom, Y., "Evaluation of the Effect of Vibration Nonlinearity on Convergence Behavior of Adaptive Higher Harmonic Control," NASA CR-166424, 1983.

[2]Nagrath, I. J., and Gopal, M., *Control Systems Engineering*, Prentice–Hall, Englewood Cliffs, NJ, 1982.

[3]Ha, C. M., "Neural Networks Approach to AIAA Aircraft Control Design Challenge," *Journal of Guidance, Control, and Dynamics*, Vol. 18, No. 4, 1995, pp. 731–739.

[4]Utkin, V. I., "Variable Structure Systems with Sliding Modes," *IEEE Transactions on Automatic Control*, Vol. 22, No. 2, 1977, pp. 212–222.

[5]Young, J.-S., and Lin, C. E., "Refined H^∞-Optimal Approach to Rotorcraft Flight Control," *Journal of Guidance, Control, and Dynamics*, Vol. 16, No. 2, 1993, pp. 247–255.

[6]Ku, C.-S., "Multidisciplinary Design of Adaptive Neurocontrollers for Vibration Reduction in Aeroelastic Systems," Ph.D. Dissertation, Dept. of Mechanical Engineering, Aeronautical Engineering and Mechanics, Rensselaer Polytechnic Inst., Troy, NY, 1997.

[7]Tseng, S. P., "Design Optimization of Lifting Surfaces Using Trailing-Edge Control Surface with Feedback Control," Ph.D. Dissertation, Dept. of Mechanical Engineering, Aeronautical Engineering and Mechanics, Rensselaer Polytechnic Inst., Troy, NY, 1994.

[8]Tran, C. T., and Petot, D., "Semi-Empirical Model for the Dynamic Stall of Airfoils in View of the Application to the Calculation of Responses of a Helicopter Blade in Forward Flight," *Sixth European Rotorcraft and Power Lift Aircraft Forum*, 1980, pp. 1–23 (Paper 48).

[9]Johnson, W., *Helicopter Theory*, Princeton Univ. Press, Princeton, NJ, 1980, Chap. 16.

[10]He, C. J., and Du Val, R. W., "An Unsteady Airload Model with Dynamic Stall for Rotorcraft Simulation," *Proceedings of the 50th Annual Forum of the American Helicopter Society* (Washington, DC), American Helicopter Society, 1994, pp. 931–948.

[11]Venkatesan, C., and Friedmann, P. P., "New Approach to Finite-State Modeling of Unsteady Aerodynamics," *AIAA Journal*, Vol. 24, No. 12, 1986, pp. 1889–1897.

[12]Theodorsen, T., "General Theory of Aerodynamic Instability and the Mechanism of Flutter," NACA Rept. 496, 1935, pp. 158–178.

[13]Hajela, P., and Berke, L., "Neural Network Based Decomposition in Optimal Structural Synthesis," *Computing Systems in Engineering*, Vol. 2, No. 5/6, 1991, pp. 473–481.

[14]Yamada, T., and Yabuta, T., "Neural Network Controller Using Autotuning Method for Nonlinear Functions," *IEEE Transactions on Neural Networks*, Vol. 3, No. 4, 1992, pp. 595–601.

[15]Takahashi, M. D., and Friedmann, P. P., "Helicopter Air Resonance Modeling and Suppression Using Active Control," *Journal of Guidance, Control, and Dynamics*, Vol. 14, No. 6, 1991, pp. 1294–1300.

[16]Ku, C.-S., and Hajela, P., "Integrated Design of an Adaptive Neurocontroller for a 2-D Aeroelastic System," *Journal of Structural Optimization*, Vol. 13, No. 2/3, 1997, pp. 172–181.

R. K. Kapania
Associate Editor